



An Automated Platform for Assessment of Congenital and Drug-Induced Arrhythmia with hiPSC-Derived Cardiomyocytes

Wesley L. McKeithan^{1,2}, Alex Savchenko¹, Michael S. Yu^{3,4}, Fabio Cerignoli^{5†}, Arne A. N. Bruyneel¹, Jeffery H. Price⁵, Alexandre R. Colas³, Evan W. Miller⁶, John R. Cashman⁷ and Mark Mercola^{1*}

¹ Department of Medicine, Cardiovascular Institute, Stanford University, Stanford, CA, United States, ² Graduate School of Biomedical Sciences, Sanford Burnham Prebys Medical Discovery Institute, La Jolla, CA, United States, ³ Sanford Burnham Prebys Medical Discovery Institute, La Jolla, CA, United States, ⁴ Department of Bioengineering, University of California, San Diego, San Diego, CA, United States, ⁵ Vala Sciences, San Diego, CA, United States, ⁶ Departments of Chemistry, Molecular and Cell Biology, Helen Wills Neuroscience, University of California, Berkeley, Berkeley, CA, United States, ⁷ Human BioMolecular Research Institute, San Diego, CA, United States

OPEN ACCESS

Edited by:

Carol Ann Remme,
University of Amsterdam, Netherlands

Reviewed by:

Christopher George,
Swansea University, United Kingdom
Simona Casini,
Zorg Academic Medical Center,
Netherlands

*Correspondence:

Mark Mercola
mmercola@stanford.edu

† Present Address:

Fabio Cerignoli,
ACEA Biosciences, San Diego, CA,
United States

Specialty section:

This article was submitted to
Cardiac Electrophysiology,
a section of the journal
Frontiers in Physiology

Received: 29 April 2017

Accepted: 19 September 2017

Published: 11 October 2017

Citation:

McKeithan WL, Savchenko A, Yu MS, Cerignoli F, Bruyneel AAN, Price JH, Colas AR, Miller EW, Cashman JR and Mercola M (2017) An Automated Platform for Assessment of Congenital and Drug-Induced Arrhythmia with hiPSC-Derived Cardiomyocytes. *Front. Physiol.* 8:766. doi: 10.3389/fphys.2017.00766

The ability to produce unlimited numbers of human induced pluripotent stem cell derived cardiomyocytes (hiPSC-CMs) harboring disease and patient-specific gene variants creates a new paradigm for modeling congenital heart diseases (CHDs) and predicting proarrhythmic liabilities of drug candidates. However, a major roadblock to implementing hiPSC-CM technology in drug discovery is that conventional methods for monitoring action potential (AP) kinetics and arrhythmia phenotypes *in vitro* have been too costly or technically challenging to execute in high throughput. Herein, we describe the first large-scale, fully automated and statistically robust analysis of AP kinetics and drug-induced proarrhythmia in hiPSC-CMs. The platform combines the optical recording of a small molecule fluorescent voltage sensing probe (VoltageFluor2.1.Cl), an automated high throughput microscope and automated image analysis to rapidly generate physiological measurements of cardiomyocytes (CMs). The technique can be readily adapted on any high content imager to study hiPSC-CM physiology and predict the proarrhythmic effects of drug candidates.

Keywords: induced pluripotent stem cells, cardiomyocyte, voltage sensitive probe, high throughput screening, drug development, cardiotoxicity, CiPA

INTRODUCTION

Between 1991 and 2003, 6 drugs were withdrawn from the market in the U.S. because of evidence that they induced QT prolongation and the potentially fatal ventricular tachycardia (VT), Torsade de Pointes (TdP) (Waring et al., 2015). At a cellular level, drug-induced VT is precipitated most commonly by drug inhibition of the human ether-à-go-go (hERG) channel. hERG conducts the rapidly activating component of the delayed rectifier potassium current (I_{Kr}) that is responsible for the bulk of ventricular repolarization. Following regulatory agency guidelines, the *in vitro* measurement of hERG inhibition has become essential for advancement of a drug candidate to clinical development (Waring et al., 2015). While the results of hERG inhibition studies have kept

dangerous drugs from reaching the market, it is poorly predictive of the development of TdP. Many drugs can inhibit hERG without causing VT or TdP (Redfern et al., 2003; Kramer et al., 2013) and some drugs can cause VT or TdP by other mechanisms (Roden, 1998; Lacerda et al., 2008). Moreover, hERG inhibition is highly sensitive to a wide range of chemical substructures (Sanguinetti and Tristani-Firouzi, 2006) that might comprise clinically beneficial components of small molecule drugs. There is considerable concern that reliance on hERG inhibition alone may prevent many useful compounds from advancing toward the clinic. This concern was embodied in the 2013 Food and Drug Administration recognition of the need for a comprehensive non-clinical assay to better predict the proarrhythmic potential of new drugs (Comprehensive *in vitro* Proarrhythmia Assay (CiPA) initiative) (Sager et al., 2014).

hiPSC-CMs are an emerging model to advance the field beyond using hERG or other single ion channels in heterologous expression systems as an *in vitro* tool to predict arrhythmogenic potential (Liang et al., 2013; Mercola et al., 2013). Other studies have shown that hiPSC-CMs express most of the ion channels of ventricular CMs and can be produced in limitless quantities from normal individuals as well as from patients with arrhythmia proclivity (Ma et al., 2011). This unique property creates an unprecedented opportunity to gain insight into drug responses on a range of genetically diverse individuals during the early stages of drug development. In addition, hiPSC-CMs make it possible to determine if certain naturally occurring polymorphisms in ion channels, discovered by genome wide association studies (GWAS) or incidentally by DNA sequencing, increase susceptibility to adverse drug responses.

To accommodate the demand to rapidly and quantitatively assess preclinical candidates through dose ranges and to evaluate genetically diverse hiPSC-CM models, we developed an automated platform to optically assess AP kinetics and quantify cellular arrhythmia phenotypes. The 384-well format assay described herein combines a small molecule voltage sensitive probe (VSP), VoltageFluor2.1.Cl (VF2.1.Cl) (Miller et al., 2012), and an automated high speed/high resolution microscope to generate AP kinetic measurements from optical recordings of CMs. Initially, we validated the assay conditions using primary rat atrial and ventricular CMs, and visualized chamber-specific drug effects. Next, we characterized the functionality of voltage-gated ion channels and β -adrenergic receptors expressed on the membrane of hiPSC-CMs with a panel of reference compounds. Furthermore, using molecules known to inhibit hERG and cause clinically relevant arrhythmia, we observed a dose-dependent drug induction of early after depolarizations (EADs) that are cellular manifestations of T-wave prolongation and premature ventricular contractions (PVCs) on the electrocardiogram (ECG). Finally, using a genetic model of congenital Long QT syndrome type 3 (LQTS3) and pharmacological models of LQTS2 and LQTS3, both of which predispose patients to VT and sudden death, we demonstrated the reversion of these disease phenotypes in a 384-well multi-well format assay. We conclude that the screening platform described herein makes it possible to comprehensively evaluate the proarrhythmic potential of many compounds in hiPSC-CMs

derived from multiple patients, demonstrating the feasibility of utilizing hiPSC-CMs and physiological screening during early stage drug development.

MATERIALS AND METHODS

Isolation of Rat Cardiomyocytes

Neonatal atrial and ventricular rat cardiomyocytes were isolated with the neonatal rat cardiomyocyte isolation kit (Worthington, New Jersey, USA) (Toraason et al., 1989; Macgregor et al., 1995) and cultured at 37°C with 5% CO₂. Briefly, heart atria and ventricles were dissected from 1 day old Hsd:Sprague–Dawley rats, then digested overnight at 4°C with trypsin. Digestion continued 12 h later with collagenase for approximately 90 min at 37°C. Isolated cells were pre-plated for 120 min on uncoated cell culture dishes to remove fibroblasts, and subsequently, atrial and ventricular cardiomyocytes were either pooled or separately seeded on Matrigel-coated 96-Well Glass-Bottom Plates (SensioPlate™, Greiner Bio-One, North Carolina, USA) in high-serum media [DMEM/F12 (1:1), 0.2% bovine serum albumin, 3 mM sodium-pyruvate, 0.1 mM ascorbic acid, 4 mg l21 transferrin, 2 mM L-glutamine, 100 nM thyroid hormone (T3) supplemented with 10% horse serum and 5% fetal calf serum (FCS)] at a density of 4×10^5 cells/well. After 24 h, media was changed to low-serum medium (the same as above but substituting 0.25% FCS for 10% horse serum and 5% FCS). Seventy two hours after seeding the cells, they were processed for voltage imaging. All animal handling and care followed the NIH Guide for Care and Use of Laboratory Animals. The experimental protocols were approved by Institutional Animal Care and Use Committees of Sanford-Burnham-Prebys Medical Discovery Institute and Stanford University.

Culture of hiPSC-CMs

Vials of both MyCell (LQTS3) and iCell (healthy individual) Cardiomyocytes (Cellular Dynamics International, Wisconsin, USA) were thawed according to the manufacturer's specifications (see Supplementary Table 1 for lot information). A single cryovial was removed from liquid nitrogen and placed on dry ice for no more than 3 min. The vial was transferred to a 37°C water bath and incubated for 4 min. Once completely thawed, the contents were slowly transferred to a 50 mL conical vial using a 1,000 μ L pipette. 1 mL of iCell Cardiomyocyte Plating Media (iCCPM) was used to rinse the inside of the cryovial to gather any remaining cells. After rinsing the vial, the 1 mL of iCCPM was added dropwise to the 50 mL conical vial over a period of 2–3 min with continuous agitation for each drop. The additional volume for dilution was calculated to achieve a final concentration of 2.5×10^5 cells/mL and depended on the specifications of each lot of cells. The additional media was added dropwise to the 50 mL vial. Once diluted, the cells were transferred into a reagent reservoir and 20 μ L was added to each well with a 16 channel pipette (Integra Viaflo II) at a flow rate of 35 μ L/s with 1 mix cycle prior to each addition in a pre-coated 384 well plate (Greiner Bio-One) with 0.1% (w/v) gelatin (Stem Cell Technologies). The plates were left standing at room temperature for 20 min to allow the cells to settle to the bottom of the plate before it was placed

in a 37°C 5% CO₂ incubator. After 24 h, the plating media was diluted by adding 80 µL of iCell Cardiomyocyte Maintenance Media (iCCMM), supplemented with 5 mM D-glucose, and subsequently 50 µL of iCCMM was removed and replaced with 50 µL of iCCMM. This process was repeated two additional times, ultimately yielding a final volume of 100 µL/well. The plates were placed back in the 37°C 5% CO₂ incubator for 48 h. Media was exchanged every other day for 14 days prior to imaging by removing 50 µL of media and adding 50 µL of fresh iCCMM.

Differentiation of hiPSCs to Cardiomyocytes

Briefly, hiPSCs (hiPSC line SCVI15; see Supplementary Table 1) were dissociated using 0.5 mM EDTA (ThermoFisher Scientific) in PBS without CaCl₂ or MgCl₂ (Corning) for 7 min at room temperature. The dissociated hiPSCs were plated at a density of 3×10^5 cells per well of a Matrigel-coated 12 well plate in mTeSR1 media (StemCell Technologies) supplemented with 2 µM Thiazovivin (Selleck Chemicals). After 24 h, the media was replaced with mTeSR1 without Thiazovivin and was replenished daily for 3–5 days until the cells reached $\geq 90\%$ confluence to begin differentiation. Cardiomyocytes were differentiated by methods previously described (Burridge et al., 2014; Cunningham et al., 2017). At day 25, cells were dissociated and plated onto Matrigel-coated 384-well tissue culture plates (Greiner Bio-One) at a density of 20,000 cells/well. All experiments were performed day 28 post-differentiation.

Preparation of VF2.1.Cl Loading Solution and Reference Compounds

VF2.1.Cl (the dye used in this study was synthesized by EWM, but is marketed as Fluovolt) dye loading solution and the compound dilutions were prepared prior to manipulation of the cells on the day of imaging. 1 µL of 2 mM VF2.1.Cl in DMSO was mixed with 1 µL of 10% Pluronic F127 (diluted in water) in a 1.7 mL tube by agitating and centrifuging 3 times. Mixing of VF2.1.Cl with Pluronic F127 prior to subsequent dilution in physiological buffer is critical for VF2.1.Cl loading. Separately, Hoechst 33258 was diluted into Tyrode's solution (136 mM NaCl, 5 mM KCl, 2 mM CaCl₂, 1 mM MgCl₂, 10 mM glucose, 10 mM HEPES, pH 7.4) to a concentration of 4 µg/mL. 1 mL of the Hoechst/Tyrode's solution was added to the 1.7 mL tube containing the VF2.1.Cl/Pluronic F127 mixture and vortexed for 10 s. The contents of the 1.7 mL tube was added to 4 mL of Hoechst/Tyrode's solution. The mixture (5 mL of a 2x concentrated VF2.1.Cl dye loading solution) can be scaled to larger volumes if reagent ratios are maintained. Reference compounds isoproterenol (Tocris, Bristol, UK), propranolol (Tocris, Bristol, UK), verapamil (Tocris, Bristol, UK), tetradotoxin (Tocris, Bristol, UK), ATX-II (Sigma Aldrich, Missouri, USA), mexiletine (Toronto Research Chemical, Toronto, Canada), ranolazine (Tocris, Bristol, UK), acetylcholine (Sigma Aldrich, Missouri, USA) and sotalol (Tocris, Bristol, UK) were diluted in water and formoterol (Tocris, Bristol, UK), isradipine (Tocris, Bristol, UK), BayK

8644 (Tocris, Bristol, UK), veratridine (Tocris, Bristol, UK), E-4031 (Tocris, Bristol, UK), and dofetilide (Tocris, Bristol, UK) were diluted in DMSO. Each compound was diluted in Tyrode's solution to a 2x concentrated stock and was warmed to 37°C using a dry heat block prior to application to the cells.

Loading of VF2.1.Cl Dye Solution and Automated Image Acquisition

hiPSC-CMs were removed from a 37°C 5% CO₂ incubator and placed immediately into in a tissue culture cabinet on a dry heat block set to 37°C to prevent temperature fluctuation during the subsequent washing and dye loading steps. All subsequent manipulations were conducted on a 37°C dry heat block. Tyrode's solution was warmed to 37°C in a water bath. To wash the cells and remove the media, 50 µL of media was removed and replaced with 50 µL of Tyrode's solution five times using a 16 channel pipette at flow rate of 35 µL/s. After the fifth wash, 50 µL of the 2x VF2.1.Cl dye loading solution was added to each well. The plate was placed back in the 37°C 5% CO₂ incubator for 50 min. After the 50 min incubation, the cells were rinsed 4 more times by removing 50 µL of Tyrode/dye solution from the well and adding 50 µL of fresh Tyrode's solution to the well and repeating. After rinsing, the cells were placed back in a 37°C 5% CO₂ incubator for 10 min to recover. After recovery, 50 µL of solution was removed and 50 µL of 2x reference compound was added to the respective well and incubated at 37°C and 5% CO₂ for 5 min before image acquisition. Time series images were acquired automatically using the IC200 KIC instrument (Vala Sciences, California, USA) at an acquisition frequency of 100 Hz for a duration of 6.5 s or 33 Hz for 20 s, as indicated in the figure legends, with excitation wavelength of 485/20 nm and emission filter 525/30 nm using a 0.75 NA 20x Nikon Apo VC objective. A single image of the Hoechst was acquired after the time series. The optimized dye loading and imaging conditions were replicated using both a different high content imager, the ImageXpress Micro XLS platform (Molecular Devices), and hiPSC-CMs produced by a novel differentiation protocol (Cunningham et al., 2017; and Supplementary Figure 3).

Image Analysis, Physiological Parameter Calculation, and Data Analysis

The image analysis and physiological parameter calculation was conducted using commercially available Cyteseer (Vala Sciences) as previously described (Cerignoli et al., 2012; Lu et al., 2015). Briefly, the image output by Cyteseer Scanner were loaded into Cyteseer and the whole well cardiac time series algorithm was executed on the image files. The metrics analyzed by the whole well cardiac time series algorithm were beat rate, normalized area under the peak trace (normalized peak integral), and APD₂₅, APD₅₀, APD₇₅, and APD₉₀ (referring to the width of the cardiac AP at a point 25, 50, 75, and 90% respectively), from the peak to baseline amplitude. EADs were quantified automatically using the default noise threshold in the whole well cardiac time series algorithm. The algorithm determines EADs as peaks following a local minimum at a user-specified threshold above the diastolic interval minimum. Data tables were analyzed using Microsoft

Excel 2013 and dose response curves and heat maps were calculated using GraphPad Prism 7 software.

Immunohistochemistry

After live imaging using VF2.1.Cl, the neonatal CMs were fixed using 4% paraformaldehyde. After fixation, the cells were incubated with a blocking solution [10% horse serum, 0.5% Triton X-100, 0.01% gelatin in phosphate buffered saline (PBS)] for 30 min at room temperature followed by incubation with anti-Myl2 (Proteintech, cat: 10906-1-AP) or anti-Myl7 (Synaptic Systems, cat: 311 011) for 1 h at room temperature. Following incubation with the primary antibody, the cells were washed 5 times with PBS before incubation with anti-mouse Alexa Fluor 568 (ThermoFisher Scientific, A-11057) or anti-rabbit Alexa Fluor 647 (ThermoFisher Scientific, A-31573) for 1 h at room temperature. After incubation with the secondary antibody, the cells were washed 5 times with PBS and stored in a 50% glycerol (v/v) solution in PBS for subsequent imaging using the KIC.

Individual Cell Image Analysis

The single cell analysis was performed manually using ImageJ. Regions of interest (ROIs) were selected using the freehand selection tool and exported as .roi files. Using nuclear labeling from the live and fixed images, offsets for the image sets were manually determined. The ROIs were then applied to the time series images and used to generate fluorescent intensity values for each ROI in all images. The data was analyzed using Microsoft Excel 2013 and plotted using GraphPad Prism 7.

Meta-Analysis of Experimental Data

An R-script (R version 3.3.1) was developed that reads the CSV files generated by Cyteseer and amalgamates all the physiological parameters of interest into a single file. Using this dataset, we performed a meta-analysis of all experiments and determined the intra and inter thaw variability in APD₇₅ as well as the relationship between APD₇₅ and the beat rate. As a result of the non-linear relationship of APD₇₅ and the beat rate, statistical significance was determined using a sliding window (center value ± 3) to mirror experimental ranges and applying the Mann-Whitney test (using the Bonferroni criterion for multiple testing).

Whole Cell Patch Clamp Electrophysiology

Cardiac ion currents were recorded from single cardiomyocytes using the whole-cell patch-clamp method. Briefly, coverslips with cardiomyocytes were transferred into electrophysiological perfused recording chamber (RC-25-F, Warner Instruments, Hamden, CT) mounted on the stage of an inverted Olympus microscope. Patch pipettes were pulled from thin-wall borosilicate glass capillaries (CORNING 7740, 1.65 mm) with a P-2000 laser pipette puller (Sutter Instruments, California, USA) and had electrode tip resistances between 1.5 and 5.5 M Ω with access resistance of <8 M Ω for whole-cell patch recordings. Series resistance and cell capacitance were compensated to between 30 and 60% in some voltage-clamp recordings. Patch electrodes were filled with intracellular solution containing: 120 mM CsCl, 20 mM tetraethylammonium chloride (TEA-Cl), 10 mM Hepes, 2.25 mM EGTA, 1 mM CaCl₂, 2 mM MgCl₂,

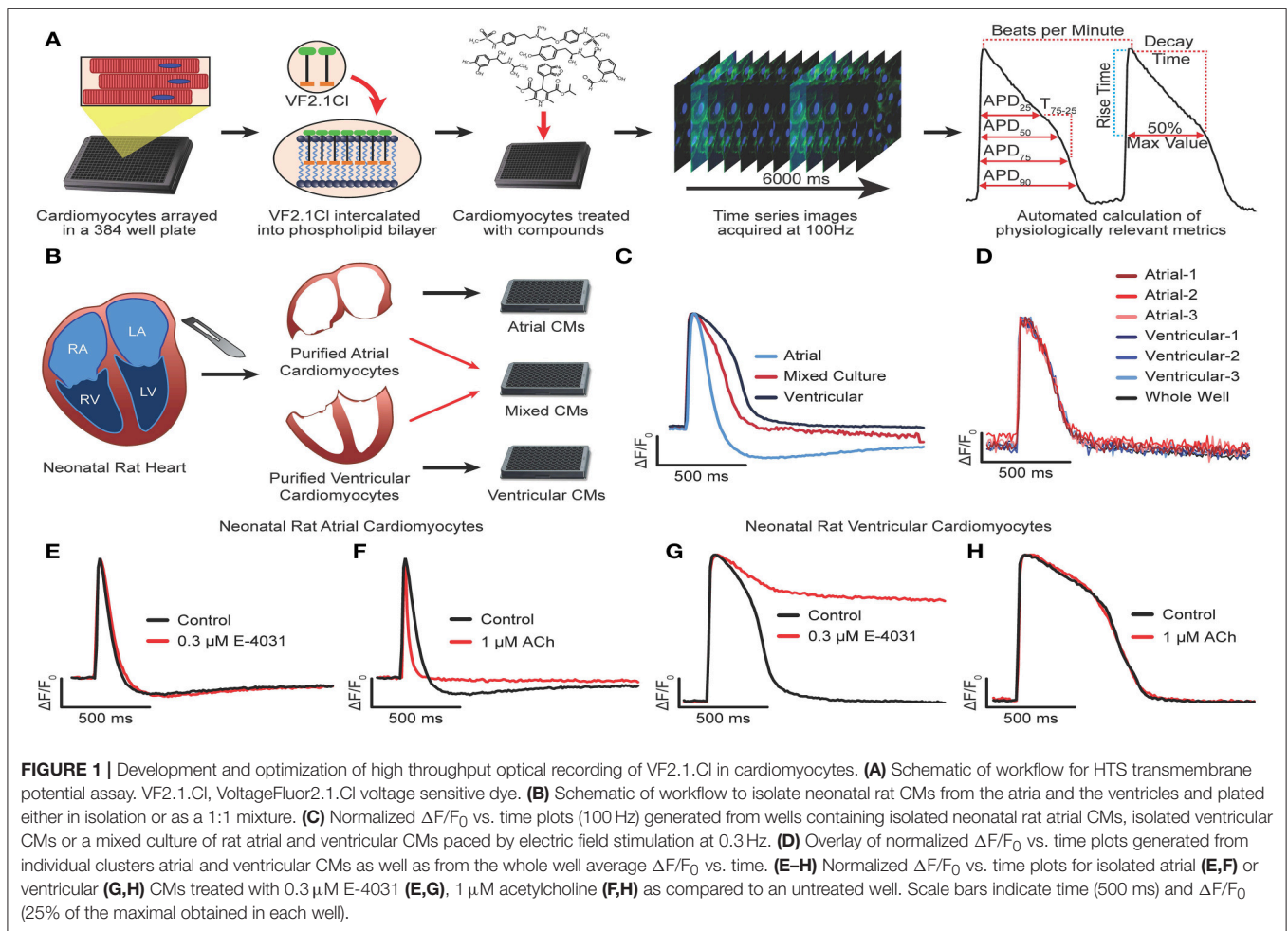
pH 7.4. All recordings were performed at room temperature in Tyrode's solution. Current response traces were acquired using the Axon 200B amplifier. Currents were digitally sampled at 10 kHz using Digidata 1322A digitizer hardware and pClamp 10.2 software (Molecular Devices, California, USA). Current responses were filtered using 8-pole Bessel analog low-pass filter at 1-2 kHz cutoff frequency. In order to record the late sodium component, the pipette-cell seal stability and access resistance was carefully monitored during the recording. Current amplitude at the end of the depolarizing step was corrected by the leak current and the corrected current amplitude was averaged for 10 cells. After the leak-correction, we computed the average value of the recorded current amplitude over the last 50 ms of the 150 ms depolarizing pulse of each 250 ms sweep and averaged the resulting value over 3 consecutive sweeps.

RESULTS

Automated Acquisition of Action Potential Kinetics with VF2.1.Cl

To create the automated platform, we developed methods for high throughput acquisition of high speed/high resolution (5.5 megapixel at 100 Hz) time series images as well as downstream image analysis to calculate physiological parameters that describe the AP kinetics of CMs in electrical syncytium (**Figure 1A**). To measure changes in membrane potential, the platform utilized VF2.1.Cl (Miller et al., 2012), which intercalates into the plasma membrane and senses changes in transmembrane potential by a novel photo-induced electron transfer (PeT) mechanism (Miller, 2016; VF2.1.Cl and related VSPs have been described in detail Woodford et al., 2015; Deal et al., 2016; Kulkarni et al., 2017, and can be obtained directly from EWM). VF2.1.Cl and structurally related probes generate a larger change in fluorescence in response to changes in voltage than conventional electrochromic dyes while maintaining sufficient time resolution to measure cardiomyocyte APs (Miller et al., 2012; Supplementary Figure 1A). We established a robust protocol to standardize cell culture conditions that consistently achieved synchronously contracting monolayers of hiPSC-CMs as well as dye loading and imaging conditions that produced optical traces with sufficient signal-to-noise and reproducibility (Supplementary Movie 1). 200 nM VF2.1.Cl and ~ 120 mW/cm² illumination intensity (excitation: 485/20 nm, emission: 525/30 nm) enabled us to achieve excellent signal-to-noise, while maintaining reproducibility (Supplementary Figure 1B). Excessive illumination or VF2.1.Cl concentration caused variability in the AP response manifested by a prolongation of the APD within successive peaks from a single recording of an individual well (Supplementary Figures 1C–K). This observation is consistent with previous reports for the VSP, di-4-ANEPPS (Schaffer et al., 1994). Thus, our optimization provided conditions for statistically robust analysis of synchronously contracting monolayers of hiPSC-CMs for high throughput screening applications.

We began development of our AP waveform analysis procedures using bona fide ventricular and atrial cardiomyocytes

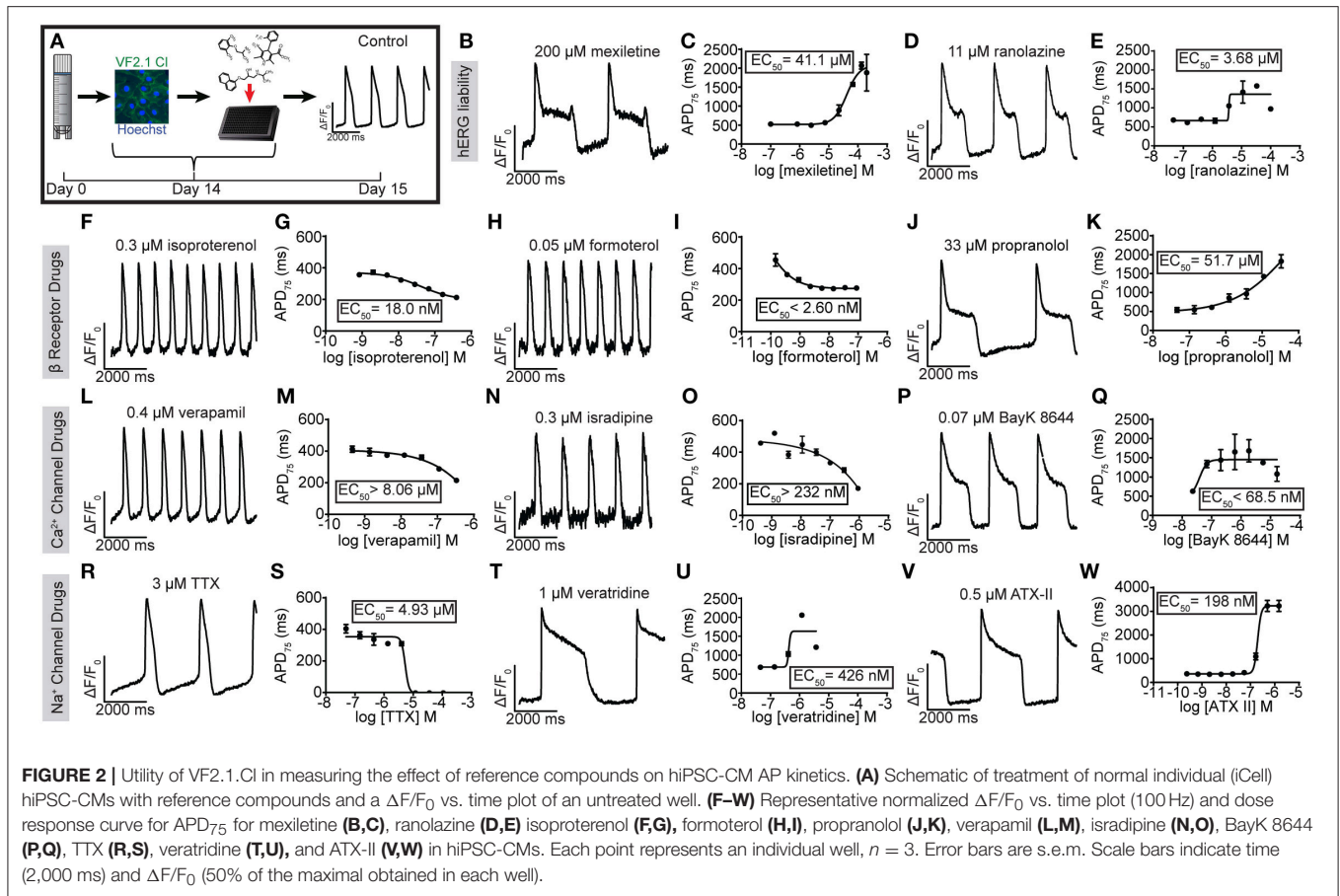


isolated from the neonatal rat heart (Figures 1B–H). Purified atrial and ventricular cardiomyocyte populations, cultured as an electrically coupled monolayer, exhibited characteristic AP morphologies using a whole well analysis (Figure 1C). However, chamber specific morphologies could not be discerned when atrial and ventricular cardiomyocytes were co-cultured in a 1:1 ratio, either at the whole well analysis, or by analyzing the waveforms of individual Myl2⁺ (ventricular) or Myl7⁺ (atrial) cardiomyocytes identified retrospectively (see Supplementary Figure 1L and Methods for overlaying waveform and immunostaining). Instead, the individual waveforms and whole well waveforms were indistinguishable (Figure 1D). In addition, no difference in AP morphology was observed in the whole well vs. individual cell waveforms of the hiPSC-CM cultures (Supplementary Figures 1M,N). These results show that AP morphology acquired from the whole well ROI represents that of all individual CMs, regardless of subtype identity, in a synchronously contracting monolayer. This result suggests that an effect on one cell type (i.e., atrial) might be masked by an opposing effect on another (i.e., ventricular) in an electrical syncytium of multiple cell types. However, whole well analysis greatly reduced the computational workload when compared to single cell analysis and enabled the rapid

generation of physiological parameters. Using this approach, we could visualize characteristic atrial specific drug effects in pure populations of neonatal rat atrial and ventricular cardiomyocytes. Acetylcholine, a selective agonist of I_{ACh} shortens the APD in atrial but not ventricular myocytes (Wang et al., 1993; Koumi et al., 1994; Devalla et al., 2015) whereas E-4031, a selective blocker of I_{Kr} mediated by hERG, prolonged APD in ventricular CMs but not atrial CMs (Figures 1E–I). Atrial CMs utilize I_{Kur} mediated by K_v1.5 in addition to I_{Kr} for repolarization, and are less sensitive hERG block (Roy et al., 1996). Thus, high throughput optical recording of VF2.1.Cl and whole well analysis was sufficient to distinguish chamber specific drug effects.

Characterization of hiPSC-CMs with Reference Compounds

The ability of hiPSC-CMs to recapitulate drug effects observed in adult CMs is critical for their use in both disease modeling and proarrhythmia evaluation. Therefore, we evaluated the expression and functionality of ion channels and adrenergic receptors with a panel of reference compounds (Figure 2A). To calculate EC₅₀ values, the cells were acutely treated with each compound (*n* = 3 wells per dose) and the average whole



well fluorescent intensity was plotted and the waveforms were used to calculate the APD_{75} for each well. Mexiletine and ranolazine are known to have an off-target inhibition of hERG, and indeed, the compounds caused a dose dependent APD prolongation and EADs at doses similar to those reported (EC_{50} of $41.1 \mu M$ and $3.68 \mu M$, respectively) (Mitcheson and Hancox, 1997; Terrenoire et al., 2013; Du et al., 2014; Galdani et al., 2015; **Figures 2B–E**, Supplementary Figures 2A,B). The non-selective β -adrenergic agonist, isoproterenol, as well as the β_2 -selective agonist, formoterol, both induced positive chronotropic responses at expected doses (EC_{50} of 18 nM and ~ 2.6 nM) (Wills et al., 2012; Sirenko et al., 2013; **Figures 2F–I**, Supplementary Figures 2C,D). The non-selective β -adrenergic antagonist, propranolol, prolonged the APD as well as slowed the beat rate considerably also as previously reported (EC_{50} of $51.7 \mu M$) (Sirenko et al., 2013; **Figures 2J,K**, Supplementary Figure 2E). The L-type calcium channel inhibitors verapamil and isradipine shortened the APD as expected and increased the beat rate (EC_{50} of $\sim 8.06 \mu M$ and ~ 232 nM) (**Figures 2L–O**, Supplementary Figures 2F,G) while the L-type calcium channel agonist, BayK 8644, significantly prolonged the APD (EC_{50} of ~ 68.5 nM) (**Figures 2P,Q**, Supplementary Figure 2H). To evaluate the presence and functionality of sodium channels in the hiPSC-CMs, the cells were treated with specific sodium channel inhibitor, tetrodotoxin (TTX), and two sodium channel agonists,

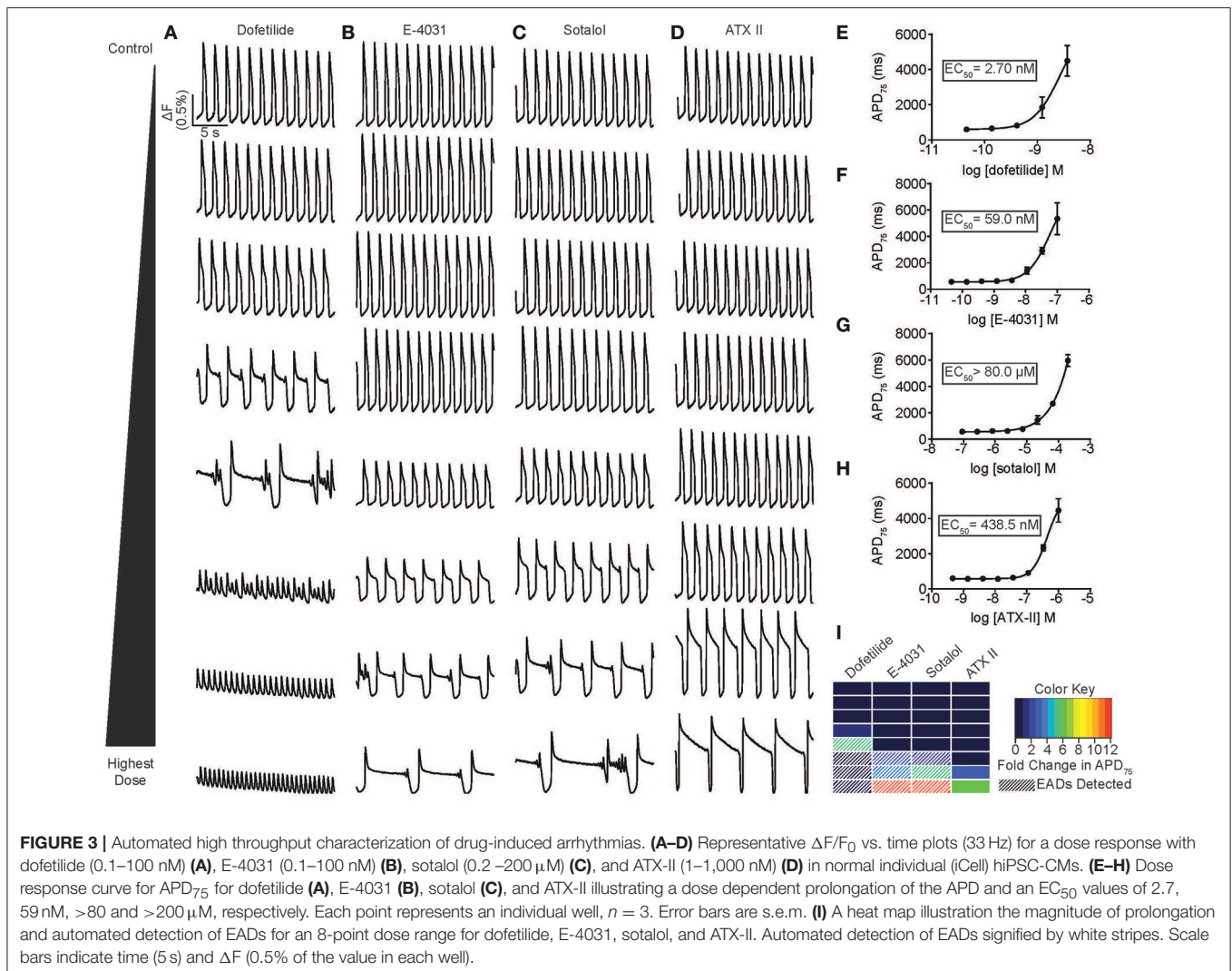
anemonia sulcata toxin (ATX-II) and veratridine, which bind to different sites on the sodium channel and open the channel by slightly different mechanisms (Stevens et al., 2011). TTX caused a cessation of beating (EC_{50} of $4.96 \mu M$) at doses comparable to the IC_{50} for peak sodium current (I_{NaP}) inhibition in CMs ($>1 \mu M$) indicating a reliance on sodium channel currents for the generation of APs (**Figures 2R,S**, Supplementary Figure 2I). However, dependence of the AP on sodium current varied across batches of CMs, suggesting inconsistency in the maturity of the hiPSC-CMs. The two sodium channel agonists prolonged the APD without inducing EADs (426 nM for veratridine and 198 nM for ATX-II) (**Figures 2T–W**, Supplementary Figures 2J,K), possibly reflecting either the maturation state of the hiPSC-CMs or genetic variation in the hiPSCs from different individuals.

To assess cross-platform reproducibility, we tested TTX, isoproterenol and E-4031 using Molecular Devices ImageXpress Micro XLS (Supplementary Figure 3, Supplementary Movies 2, 3) using iPSC-CMs prepared in-house (Cunningham et al., 2017), revealing similar dose responsiveness (EC_{50} for isoproterenol 77 nM, EC_{50} for TTX $4.85 \mu M$, EC_{50} for E-4031 >13.1 nM, EC_{50} for ATX-II $1.03 \mu M$). In summary, optical recording of hiPSC-CM AP waveform kinetics in response to reference compounds reveals the expected functional expression of cardiac ion channels (see Supplementary Table 2).

Automated Quantification of Drug-Induced Arrhythmias

The appearance of EADs and voltage alternans are the cellular manifestations of T-wave prolongation and PVCs seen on the ECG that predispose patients to VT and TdP. Therefore, we analyzed the incidence of EADs in hiPSC-CMs treated with inhibitors of I_{Kr} and an agonist of the late sodium current (I_{NaL}). The development of these morphologies can be better assessed over longer periods of recording (Mohammad et al., 1997; Song et al., 2008). Thus, time series images were acquired for 20 s at 33 Hz to provide improved signal to noise as well as recording duration, and coupled with an automated image analysis to determine the effect of the hERG blockers dofetilide, E-4031 and sotalol. All three molecules caused extensive dose-dependent prolongation of APD, induction of EADs and, at some doses, voltage alternans (Figures 3A–C, see also Supplementary Figure 3). Representative movie clips for dofetilide illustrate the presence of EADs as compared to untreated hiPSC-CMs (Supplementary Movies 4, 5), and treatment with 33 and 100 nM dofetilide caused rapidly firing subthreshold APs that

did not induce contraction (Supplementary Movies 6, 7). The appearance of these AP morphologies seemed analogous to tachyarrhythmia or fibrillation. To determine an EC_{50} dose for prolongation of the APD, dose response curves were generated from the APD_{75} values (Figures 3E–H, see also Supplementary Figure 3) in addition to the automatic detection of EADs (Figure 3I). Each of the hERG inhibitors induced significant APD prolongation as well as induced EADs at expected EC_{50} values (2.79 nM for dofetilide, 59.0 nM for E-4031 and $\sim 80 \mu\text{M}$ for sotalol). Interestingly, EADs were not detected in the ATX-II condition in the CDI hiPSC-CMs, although the compound prolonged the APD more than 7-fold (EC_{50} of 438.5 nM), which was comparable to the extent of prolongation by dofetilide and sotalol. However, we have noted EADs in other hiPSC-CM populations, most likely reflecting cell line or differentiation protocol-specific differences (Supplementary Figure 3D). In conclusion, optical recording visualized drug induced prolongation of the APD, induction of EADs as well as tachyarrhythmia *in vitro*.

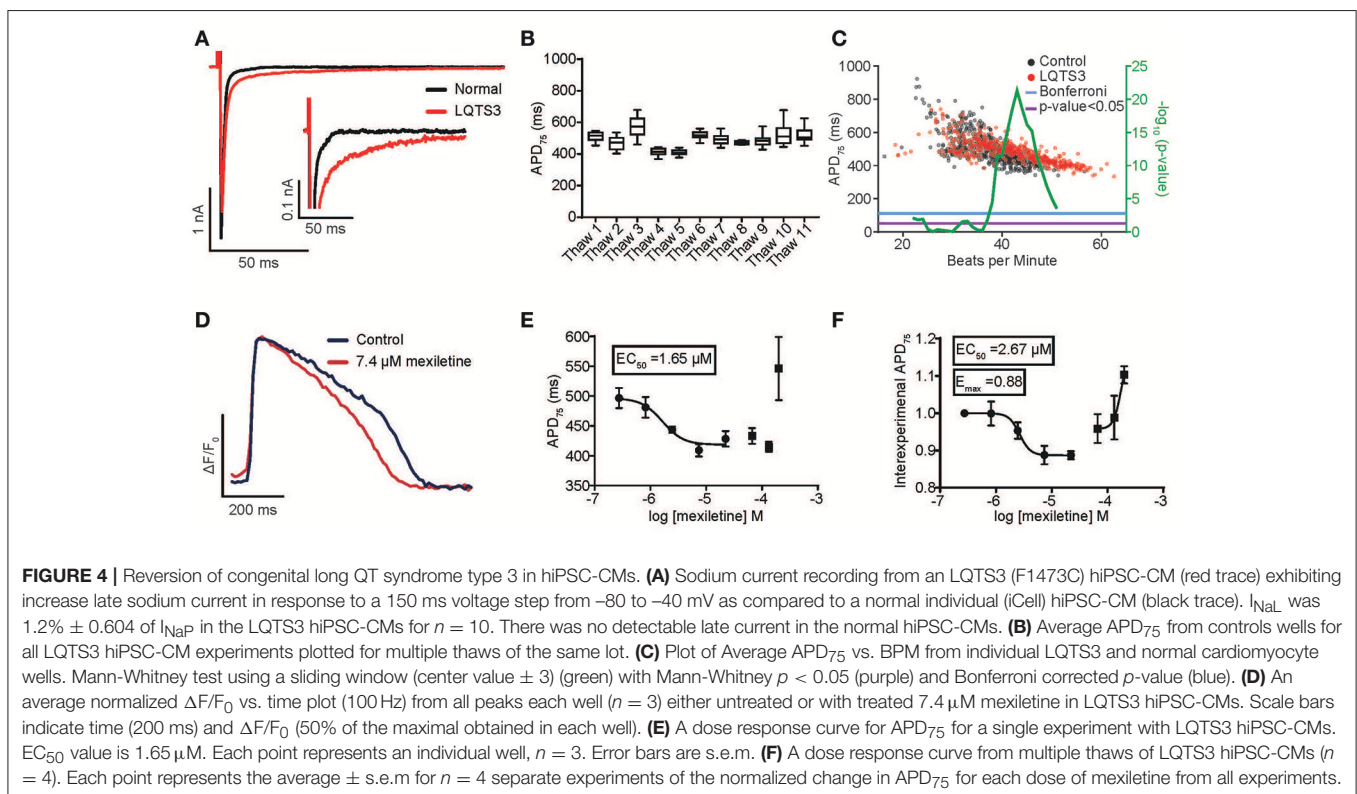


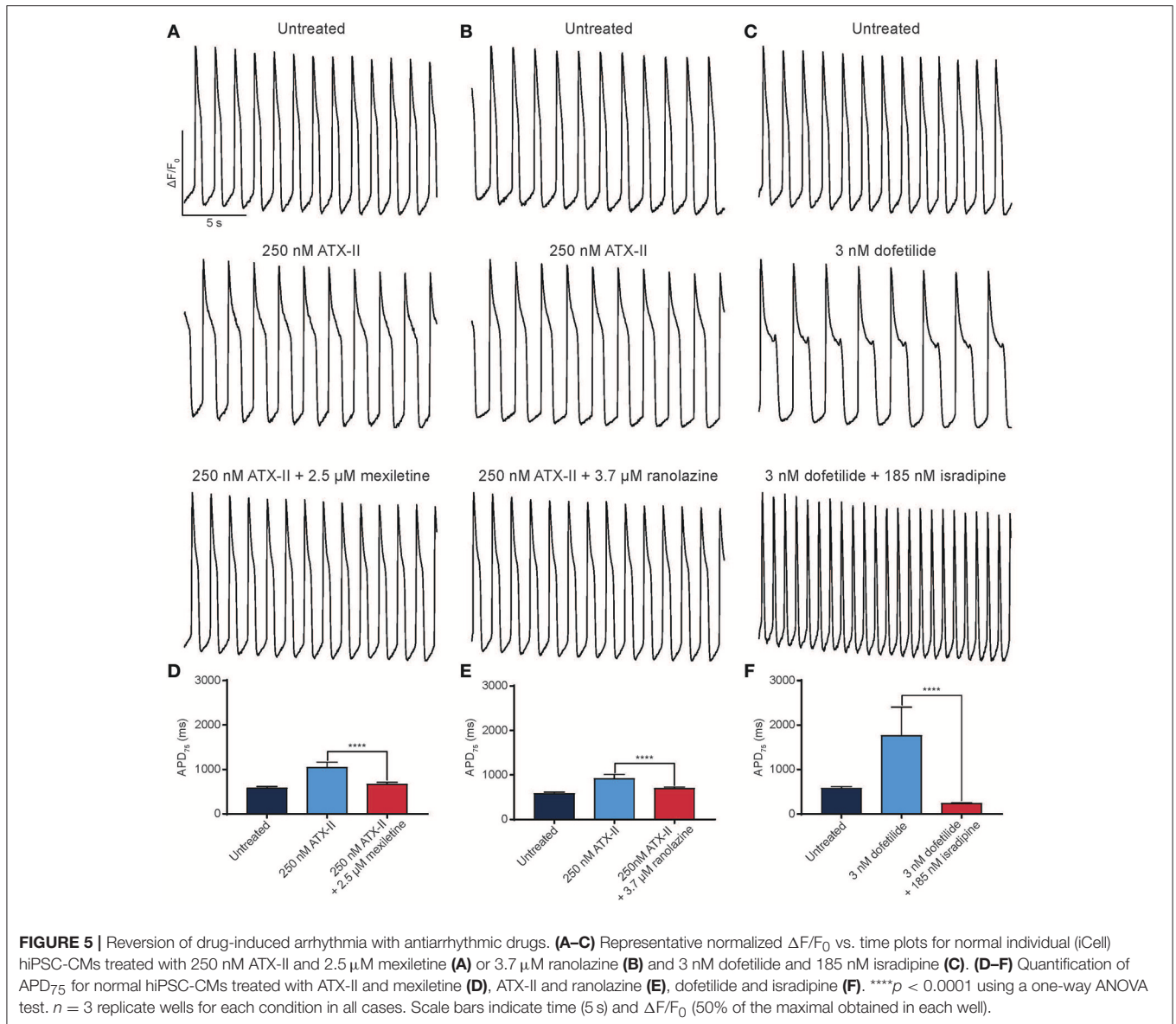
Reversion of Congenital and Drug Induced APD Prolongation

Congenital and pharmacological hiPSC-CM models of arrhythmia are of enormous interest as tools to decipher arrhythmogenic mechanisms. Moreover, an individual's genetic makeup (particularly polymorphisms in voltage-gated ion channels) can predispose patients to drug-induced arrhythmia and might underlie the sporadic nature of this phenomenon in the population (Yang et al., 2002). Therefore, visualizing drug-induced arrhythmia in hiPSC-CM models from healthy and diseased individuals is potentially a powerful new tool to personalize treatment as well as to predict liability of drug candidates across "high risk" individuals. To test this hypothesis, we evaluated a previously characterized LQTS3 patient harboring a F1473C missense mutation in the cardiac sodium channel, $I_{NaV1.5}$ (Terrenoire et al., 2013). Whole cell patch clamp recording of hiPSC-CMs derived from the LQTS3 patient confirmed increased I_{NaL} (I_{NaL} was $1.2\% \pm 0.604$ of I_{NaP} in the LQTS3 hiPSC-CMs, $n = 10$, and no detectable late current in the normal hiPSC-CMs) (Figure 4A, Supplementary Movie 8), which is a hallmark of LQTS3, indicating that the cells were a bona fide model of the congenital channelopathy. We used the high throughput platform to evaluate the reproducibility of APD across multiple preparations of LQTS3 hiPSC-CMs. Intra-experimental APDs of spontaneously beating hiPSC-CMs were very consistent with an average coefficient of variation (CV) = 0.069 ± 0.019 for untreated wells across multiple plates from the same thaw. The inter-experimental average APD

from vials thawed on different days had more variability (CV = 0.098) (Figure 4B). We plotted the average APD for every untreated, control well across all experiments and a statistically significant difference in APD between the normal and LQTS3 hiPSC-CMs was discernible only above a spontaneous beat rate of 37 beats per minute (BPM) based on the Bonferroni corrected $p < 0.05$ (Figure 4C) which is consistent with prior studies showing a phenotypic variability of the LQTS3 phenotype (Ma et al., 2013; Paci et al., in press). Nonetheless, when probed pharmacologically with mexiletine, a sodium channel inhibitor with selectivity for I_{NaL} over peak sodium current (I_{NaP}) (Wang et al., 1997), LQTS3 hiPSC-CMs showed a stereotypic, dose-dependent AP shortening, effectively reversing the LQTS3 phenotype ($EC_{50} = 1.65 \mu M$) (Figures 4D,E). This reversion was highly consistent across 4 different thaws of LQTS3 hiPSC-CMs spanning 38–53 BPM, as seen when baseline APD is normalized for each dose (average $EC_{50} = 2.67 \mu M$ and average E_{max} of 0.88) indicating a robust reversion of the disease phenotype that was independent of the variation in APD and beat rate (Figure 4F).

Pharmacological models of LQTS are commonly used to probe drug effects on APD and arrhythmia (Shimizu and Antzelevitch, 1999). LQTS3 can be modeled pharmacologically by treatment with ATX-II, which phenocopies the disease by specifically inhibiting fast inactivation of cardiac sodium channels. ATX-II-induced APD prolongation can be effectively reverted by $2.5 \mu M$ mexiletine (Figures 5A,D) and another I_{NaL} selective inhibitor ranolazine ($3.7 \mu M$) (Figures 5B,E). Finally, we created a pharmacological model of LQTS2 using the I_{Kr}





inhibitor, dofetilide. APD prolongation caused by 3 nM dofetilide was effectively reverted by 185 nM isradipine, an L-type calcium channel inhibitor (**Figures 5C,F**) (as expected because blocking the inward calcium current counteracts the block to the outward potassium current). Thus, the automated platform facilitates the characterization of diseased hiPSC-CMs and pharmacological models of disease in normal cells, and in both cases, can detect the therapeutic effect of small molecule drugs.

DISCUSSION

Using an optical method for high throughput detection of AP kinetics, we developed an automated platform for assessment of proarrhythmia in normal and channelopathy patient derived hiPSC-CMs. Our optimized procedures can be

readily implemented on automated microscopes and provides a cost effective alternative to microelectrode arrays (MEAs) with the added benefit of detecting action potentials directly rather than inferring it from extracellular field potentials. Although other methods for the quantification of arrhythmia in hiPSC-CMs have been used previously to record the electrophysiological effects of reference compounds including MEAs (Guo et al., 2011; Navarrete et al., 2013; Gilchrist et al., 2015), optogenetic methods (Dempsey et al., 2016; Klimas et al., 2016), calcium sensitive probes (Sirenko et al., 2013; Pfeiffer et al., 2016) and VSPs (Lopez-Izquierdo et al., 2014; Bedut et al., 2016; Zeng et al., 2016), our study is the first large scale, automated evaluation of reference compounds in 384 well plate format using patient-derived hiPSC-CMs by any modality, and facilitates the rapid generation of dose response curves for many physiologically relevant parameters. Moreover, our study is the first to use a VSP

to characterize a patient-specific hiPSC-CM disease model using an automated platform to quantify arrhythmia phenotypes and demonstrate reversion of those disease phenotypes with small molecule therapeutics *in vitro*.

The hiPSC-CMs presented arrhythmia phenotypes (voltage alternans, EADs, rapid APs resembling fibrillation, and cessation of beating) in response to reference compounds at expected doses. These results are consistent with previous studies indicating that hiPSC-CMs can discriminate the proarrhythmic influences of small molecules and inherited channel mutations (Matsa et al., 2011; Liang et al., 2013). By developing an assay in 384-well plate format and incorporating optical recording with automated analyses, our study advances the use of hiPSC-CMs as tools for the evaluation of arrhythmogenic potential of candidate molecules that complement conventional, lower throughput assays, such as whole animals or *ex vivo* heart preparations. In addition, hiPSC-CM technology allows individual patient backgrounds to be evaluated with greater throughput than can be achieved with conventional methods. The increased throughput enables unbiased functional genomics screening of proteins or genes (i.e., siRNAs, miRNAs or CRISPR gene knockouts) in diverse genetic backgrounds of normal and CHD patient-specific hiPSC-CMs, accelerating our ability to generate systems level insight into arrhythmia mechanisms.

Important limitations in the use of hiPSC-CMs to evaluate pro-arrhythmia include differences in ion channel physiology between these cells and adult cardiomyocytes, such as a larger I_f that confers automaticity, and reduced I_{K1} that is involved in maintaining the low resting potential of adult CMs (Del Alamo et al., 2016). Although the relatively pure and synchronously contracting monolayer hiPSC-CM cultures allow us to discern cellular arrhythmia phenotypes in the 384-well format, these cultures cannot reliably reproduce arrhythmia mechanisms that depend on complex 3D architecture of the normal or diseased heart. Additionally, we found that the ability to discern chamber specific AP waveforms as well as chamber specific drug effects required the culture of pure populations of sub type specific CMs and could not be identified through single cell analysis of our synchronously contracting monolayers. hiPSC-CM differentiation and culture methods are advancing, and recent nano and micro patterning of cell culture substrates have already improved the fidelity of the hiPSC-CMs as models of adult cardiomyocyte physiology, in particular calcium-induced calcium release, force-generation and adrenergic signaling (Kim et al., 2010; Feaster et al., 2015; Ribeiro A. J. et al., 2015; Jung et al., 2016). Such advances would improve the ability to correlate the cellular arrhythmia phenotypes recorded here with clinical arrhythmia. Key areas for further improvement include sarcomeric structural organization (Pasqualini et al., 2015) force generation (Ribeiro A. J. et al., 2015; Ribeiro M. C. et al., 2015), metabolism (Yang et al., 2014) as well as chamber subtype specific differentiation protocols (Devalla et al., 2015). In addition, while performing this study, we observed that certain hiPSC-CM batches (and differentiation protocols) yielded cells that were resistant to TTX-induced cessation of beating at the time the cells were tested. Moreover,

CMs from some hiPSC lines presented EADs in response to ATX-II (generated in-house) whereas others (i.e., iCell) did not (Figure 3D and Supplementary Figure 3D). Such variability might reflect differences in cell donors or CM differentiation protocols. TTX-resistant batches responded to ATX-II by AP prolongation, indicating that sodium channels are typically present but are inactive consistent with a relatively depolarized diastolic membrane potential (e.g., Veerman et al., 2015). Given the variability in maturation state of cardiomyocytes due to differences in time in culture as well as the protocol used to differentiate cardiomyocytes from hiPSCs, AP dependence on sodium channels should be evaluated across protocols and commercial hiPSC-CM preparations. Finally, our protocol and instrument parameters did not evaluate AP resting potential or V_{max} because of non-ratiometric nature of the VSP and the acquisition frame rate (100 frames/s), respectively, although a faster frame rate is feasible on the IC200.

In summary, hiPSC-CM technology in cardiovascular drug discovery and clinical management of heart disease is emerging as a viable paradigm. Indeed, low throughput methods have shown that it is possible to revert arrhythmia phenotypes in hiPSC-CM channelopathy models following drug treatment, and that the influence of patient genetic makeup on drug-induced arrhythmia is manifest in the cell cultures (Sharma et al., 2013). Automated 384-well plate screening enables large-scale studies that should make it possible to introduce testing of patient cells at early stages of drug development, decipher basic arrhythmia mechanisms, and test whether individual patient differences can predict clinical outcome.

AUTHOR CONTRIBUTIONS

WM, AS, MY, AC, FC, and AB conducted the experiments and analyzed the data. EM synthesized VF2.1.Cl. JP, JC, and MM obtained funding. WM and MM wrote, and everyone edited, the manuscript.

ACKNOWLEDGMENTS

We gratefully acknowledge grant support from the NIH (1R01HL132225, 1R01HL130840, 1R01HL128072, 1R01HL113601, and 1R01HL113006), Stanford University and the Fondation Leducq (Shapeheart) to MM, and from the California Institute for Regenerative Medicine (CIRM TR4-06857) to JC and MM. EM acknowledges support from UC Berkeley, NIH (R35GM119855 and R00NS078561), March of Dimes (5-FY16-65), and the Alfred P. Sloan Foundation. NIH SBIR Contract HHSN268200900044C to FC, JP, and MM. Core facilities were supported by 5P30AR061303 and 5P30CA 030199.

SUPPLEMENTARY MATERIAL

The Supplementary Material for this article can be found online at: <https://www.frontiersin.org/articles/10.3389/fphys.2017.00766/full#supplementary-material>

REFERENCES

- Bedut, S., Seminatore-Nole, C., Lamamy, V., Caignard, S., Boutin, J. A., Nosjean, O., et al. (2016). High-throughput drug profiling with voltage- and calcium-sensitive fluorescent probes in human iPSC-derived cardiomyocytes. *Am. J. Physiol. Heart Circ. Physiol.* 311, H44–H53. doi: 10.1152/ajpheart.00793.2015
- Burridge, P. W., Matsa, E., Shukla, P., Lin, Z. C., Churko, J. M., Ebert, A. D., et al. (2014). Chemically defined generation of human cardiomyocytes. *Nat. Methods* 11, 855–860. doi: 10.1038/nmeth.2999
- Cerignoli, F., Charlot, D., Whittaker, R., Ingermanson, R., Gehalot, P., Savchenko, A., et al. (2012). High throughput measurement of $Ca^{2(+)}$ dynamics for drug risk assessment in human stem cell-derived cardiomyocytes by kinetic image cytometry. *J. Pharmacol. Toxicol. Methods* 66, 246–256. doi: 10.1016/j.vascn.2012.08.167
- Cunningham, T. J., Yu, M. S., McKeithan, W. L., Spiering, S., Carrette, F., Huang, C.-T., et al. (2017). Id genes are essential for early heart formation. *Genes Dev.* 31, 1325–1338. doi: 10.1101/gad.300400.117
- Deal, P. E., Kulkarni, R. U., Al-Abdullatif, S. H., and Miller, E. W. (2016). Isomerically pure tetramethylrhodamine voltage reporters. *J. Am. Chem. Soc.* 138, 9085–9088. doi: 10.1021/jacs.6b05672
- Del Alamo, J. C., Lemons, D., Serrano, R., Savchenko, A., Cerignoli, F., Bodmer, R., et al. (2016). High throughput physiological screening of iPSC-derived cardiomyocytes for drug development. *Biochim. Biophys. Acta* 1863, 1717–1727. doi: 10.1016/j.bbamcr.2016.03.003
- Dempsey, G. T., Chaudhary, K. W., Atwater, N., Nguyen, C., Brown, B. S., McNeish, J. D., et al. (2016). Cardiotoxicity screening with simultaneous optogenetic pacing, voltage imaging and calcium imaging. *J. Pharmacol. Toxicol. Methods* 81, 240–250. doi: 10.1016/j.vascn.2016.05.003
- Devalla, H. D., Schwach, V., Ford, J. W., Milnes, J. T., El-Haou, S., Jackson, C., et al. (2015). Atrial-like cardiomyocytes from human pluripotent stem cells are a robust preclinical model for assessing atrial-selective pharmacology. *EMBO Mol. Med.* 7, 394–410. doi: 10.15252/emmm.201404757
- Du, C., Zhang, Y., El Harchi, A., Dempsey, C. E., and Hancox, J. C. (2014). Ranolazine inhibition of hERG potassium channels: drug-pore interactions and reduced potency against inactivation mutants. *J. Mol. Cell. Cardiol.* 74, 220–230. doi: 10.1016/j.yjmcc.2014.05.013
- Feaster, T. K., Cadar, A. G., Wang, L., Williams, C. H., Chun, Y. W., Hempel, J. E., et al. (2015). Matrigel mattress: a method for the generation of single contracting human-induced pluripotent stem cell-derived cardiomyocytes. *Circ. Res.* 117, 995–1000. doi: 10.1161/CIRCRESAHA.115.307580
- Gilchrist, K. H., Lewis, G. F., Gay, E. A., Sellgren, K. L., and Grego, S. (2015). High-throughput cardiac safety evaluation and multi-parameter arrhythmia profiling of cardiomyocytes using microelectrode arrays. *Toxicol. Appl. Pharmacol.* 288, 249–257. doi: 10.1016/j.taap.2015.07.024
- Gualdani, R., Tadini-Buoninsegni, F., Roselli, M., Defrenza, I., Contino, M., Colabufo, N. A., et al. (2015). Inhibition of hERG potassium channel by the antiarrhythmic agent mexiletine and its metabolite m-hydroxymexiletine. *Pharmacol. Res. Perspect.* 3:e00160. doi: 10.1002/prp2.160
- Guo, L., Abrams, R. M., Babiarz, J. E., Cohen, J. D., Kameoka, S., Sanders, M. J., et al. (2011). Estimating the risk of drug-induced proarrhythmia using human induced pluripotent stem cell-derived cardiomyocytes. *Toxicol. Sci.* 123, 281–289. doi: 10.1093/toxsci/kfr158
- Jung, G., Fajardo, G., Ribeiro, A. J., Kooiker, K. B., Coronado, M., Zhao, M., et al. (2016). Time-dependent evolution of functional vs. remodeling signaling in induced pluripotent stem cell-derived cardiomyocytes and induced maturation with biomechanical stimulation. *FASEB J.* 30, 1464–1479. doi: 10.1096/fj.15-280982
- Kim, D. H., Lipke, E. A., Kim, P., Cheong, R., Thompson, S., Delannoy, M., et al. (2010). Nanoscale cues regulate the structure and function of macroscopic cardiac tissue constructs. *Proc. Natl. Acad. Sci. U.S.A.* 107, 565–570. doi: 10.1073/pnas.0906504107
- Klimas, A., Ambrosi, C. M., Yu, J., Williams, J. C., Bien, H., and Entcheva, E. (2016). OptoDyCE as an automated system for high-throughput all-optical dynamic cardiac electrophysiology. *Nat. Commun.* 7:11542. doi: 10.1038/ncomms11542
- Koumi, S., Arentzen, C. E., Backer, C. L., and Wasserstrom, J. A. (1994). Alterations in muscarinic K^+ channel response to acetylcholine and to G protein-mediated activation in atrial myocytes isolated from failing human hearts. *Circulation* 90, 2213–2224. doi: 10.1161/01.CIR.90.5.2213
- Kramer, J., Obejero-Paz, C. A., Myatt, G., Kuryshev, Y. A., Bruening-Wright, A., Verducci, J. S., et al. (2013). MICE models: superior to the HERG model in predicting Torsade de Pointes. *Sci. Rep.* 3:2100. doi: 10.1038/srep02100
- Kulkarni, R. U., Kramer, D. J., Pourmandi, N., Karbasi, K., Bateup, H. S., and Miller, E. W. (2017). Voltage-sensitive rhodol with enhanced two-photon brightness. *Proc. Natl. Acad. Sci. U.S.A.* 114, 2813–2818. doi: 10.1073/pnas.1610791114
- Lacerda, A. E., Kuryshev, Y. A., Chen, Y., Renganathan, M., Eng, H., Danthi, S. J., et al. (2008). Alifuzosin delays cardiac repolarization by a novel mechanism. *J. Pharmacol. Exp. Ther.* 324, 427–433. doi: 10.1124/jpet.107.128405
- Liang, P., Lan, F., Lee, A. S., Gong, T., Sanchez-Freire, V., Wang, Y., et al. (2013). Drug screening using a library of human induced pluripotent stem cell-derived cardiomyocytes reveals disease-specific patterns of cardiotoxicity. *Circulation* 127, 1677–1691. doi: 10.1161/CIRCULATIONAHA.113.001883
- Lopez-Izquierdo, A., Warren, M., Riedel, M., Cho, S., Lai, S., Lux, R. L., et al. (2014). A near-infrared fluorescent voltage-sensitive dye allows for moderate-throughput electrophysiological analyses of human induced pluripotent stem cell-derived cardiomyocytes. *Am. J. Physiol. Heart Circ. Physiol.* 307, H1370–H1377. doi: 10.1152/ajpheart.00344.2014
- Lu, H. R., Whittaker, R., Price, J. H., Vega, R., Pfeiffer, E. R., Cerignoli, F., et al. (2015). High throughput measurement of Ca^{++} dynamics in human stem cell-derived cardiomyocytes by kinetic image cytometry: a cardiac risk assessment characterization using a large panel of cardioactive and inactive compounds. *Toxicol. Sci.* 148, 503–516. doi: 10.1093/toxsci/kfv201
- Ma, D., Wei, H., Zhao, Y., Lu, J., Li, G., Sahib, N. B., et al. (2013). Modeling type 3 long QT syndrome with cardiomyocytes derived from patient-specific induced pluripotent stem cells. *Int. J. Cardiol.* 168, 5277–5286. doi: 10.1016/j.ijcard.2013.08.015
- Ma, J., Guo, L., Fiene, S. J., Anson, B. D., Thomson, J. A., Kamp, T. J., et al. (2011). High purity human-induced pluripotent stem cell-derived cardiomyocytes: electrophysiological properties of action potentials and ionic currents. *Am. J. Physiol. Heart Circ. Physiol.* 301, H2006–H2017. doi: 10.1152/ajpheart.00694.2011
- Macgregor, R. R., Klein, R. M., and Bansal, D. D. (1995). Secretion of plasminogen activator activity from neonatal rat heart cells is regulated by hormones and growth factors. *Ann. N.Y. Acad. Sci.* 752, 331–342. doi: 10.1111/j.1749-6632.1995.tb17442.x
- Matsa, E., Rajamohan, D., Dick, E., Young, L., Mellor, I., Staniforth, A., et al. (2011). Drug evaluation in cardiomyocytes derived from human induced pluripotent stem cells carrying a long QT syndrome type 2 mutation. *Eur. Heart J.* 32, 952–962. doi: 10.1093/eurheartj/ehr073
- Mercola, M., Colas, A., and Willems, E. (2013). Induced pluripotent stem cells in cardiovascular drug discovery. *Circ. Res.* 112, 534–548. doi: 10.1161/CIRCRESAHA.111.250266
- Miller, E. W. (2016). Small molecule fluorescent voltage indicators for studying membrane potential. *Curr. Opin. Chem. Biol.* 33, 74–80. doi: 10.1016/j.cbpa.2016.06.003
- Miller, E. W., Lin, J. Y., Frady, E. P., Steinbach, P. A., Kristan, W. B. Jr., and Tsien, R. Y. (2012). Optically monitoring voltage in neurons by photo-induced electron transfer through molecular wires. *Proc. Natl. Acad. Sci. U.S.A.* 109, 2114–2119. doi: 10.1073/pnas.1120694109
- Mitcheson, J. S., and Hancox, J. C. (1997). Modulation by mexiletine of action potentials, L-type Ca current and delayed rectifier K current recorded from isolated rabbit atrioventricular nodal myocytes. *Pflugers Arch.* 434, 855–858. doi: 10.1007/s004240050476
- Mohammad, S., Zhou, Z., Gong, Q., and January, C. T. (1997). Blockage of the HERG human cardiac K^+ channel by the gastrointestinal prokinetic agent cisapride. *Am. J. Physiol.* 273, H2534–H2538.
- Navarrete, E. G., Liang, P., Lan, F., Sanchez-Freire, V., Simmons, C., Gong, T., et al. (2013). Screening drug-induced arrhythmia [corrected] using human induced pluripotent stem cell-derived cardiomyocytes and low-impedance microelectrode arrays. *Circulation* 128, S3–S13. doi: 10.1161/CIRCULATIONAHA.112.000570
- Paci, M., Passini, E., Severi, S., Hyttinen, J., and Rodriguez, B. (in press). Phenotypic variability in LQT3 human induced pluripotent stem cell-derived cardiomyocytes and their response to antiarrhythmic pharmacologic therapy: an *in silico* approach. *Heart Rhythm.* doi: 10.1016/j.hrthm.2017.07.026

- Pasqualini, F. S., Sheehy, S. P., Agarwal, A., Aratyn-Schaus, Y., and Parker, K. K. (2015). Structural phenotyping of stem cell-derived cardiomyocytes. *Stem Cell Rep.* 4, 340–347. doi: 10.1016/j.stemcr.2015.01.020
- Pfeiffer, E. R., Vega, R., McDonough, P. M., Price, J. H., and Whittaker, R. (2016). Specific prediction of clinical QT prolongation by kinetic image cytometry in human stem cell derived cardiomyocytes. *J. Pharmacol. Toxicol. Methods* 81, 263–273. doi: 10.1016/j.vascn.2016.04.007
- Redfern, W. S., Carlsson, L., Davis, A. S., Lynch, W. G., Mackenzie, I., Palethorpe, S., et al. (2003). Relationships between preclinical cardiac electrophysiology, clinical QT interval prolongation and torsade de pointes for a broad range of drugs: evidence for a provisional safety margin in drug development. *Cardiovasc. Res.* 58, 32–45. doi: 10.1016/S0008-6363(02)00846-5
- Ribeiro, A. J., Ang, Y. S., Fu, J. D., Rivas, R. N., Mohamed, T. M., Higgs, G. C., et al. (2015). Contractility of single cardiomyocytes differentiated from pluripotent stem cells depends on physiological shape and substrate stiffness. *Proc. Natl. Acad. Sci. U.S.A.* 112, 12705–12710. doi: 10.1073/pnas.1508073112
- Ribeiro, M. C., Tertoolen, L. G., Guadix, J. A., Bellin, M., Kosmidis, G., D'aniello, C., et al. (2015). Functional maturation of human pluripotent stem cell derived cardiomyocytes *in vitro*—correlation between contraction force and electrophysiology. *Biomaterials* 51, 138–150. doi: 10.1016/j.biomaterials.2015.01.067
- Roden, D. M. (1998). Mechanisms and management of proarrhythmia. *Am. J. Cardiol.* 82, 49I–57I. doi: 10.1016/S0002-9149(98)00472-X
- Roy, M., Dumaine, R., and Brown, A. M. (1996). HERG, a primary human ventricular target of the non-sedating antihistamine terfenadine. *Circulation* 94, 817–823. doi: 10.1161/01.CIR.94.4.817
- Sager, P. T., Gintant, G., Turner, J. R., Pettit, S., and Stockbridge, N. (2014). Rechanneling the cardiac proarrhythmia safety paradigm: a meeting report from the Cardiac Safety Research Consortium. *Am. Heart J.* 167, 292–300. doi: 10.1016/j.ahj.2013.11.004
- Sanguinetti, M. C., and Tristani-Firouzi, M. (2006). hERG potassium channels and cardiac arrhythmia. *Nature* 440, 463–469. doi: 10.1038/nature04710
- Schaffer, P., Ahammer, H., Muller, W., Koidl, B., and Windisch, H. (1994). Di-4-ANEPPS causes photodynamic damage to isolated cardiomyocytes. *Pflugers Arch.* 426, 548–551. doi: 10.1007/BF00378533
- Sharma, A., Wu, J. C., and Wu, S. M. (2013). Induced pluripotent stem cell-derived cardiomyocytes for cardiovascular disease modeling and drug screening. *Stem Cell Res. Ther.* 4, 150. doi: 10.1186/scrt380
- Shimizu, W., and Antzelevitch, C. (1999). Differential response of transmural dispersion of repolarization and torsade de pointes to beta-adrenergic agonists and antagonists in three models of the long QT syndrome. *J. Electrocardiol.* 32(Suppl.), 150. doi: 10.1016/S0022-0736(99)90065-1
- Sirenko, O., Crittenden, C., Callamaras, N., Hesley, J., Chen, Y. W., Funes, C., et al. (2013). Multiparameter *in vitro* assessment of compound effects on cardiomyocyte physiology using iPSC cells. *J. Biomol. Screen.* 18, 39–53. doi: 10.1177/1087057112457590
- Song, Y., Shryock, J. C., and Belardinelli, L. (2008). An increase of late sodium current induces delayed afterdepolarizations and sustained triggered activity in atrial myocytes. *Am. J. Physiol. Heart Circ. Physiol.* 294, H2031–H2039. doi: 10.1152/ajpheart.01357.2007
- Stevens, M., Peigneux, S., and Tytgat, J. (2011). Neurotoxins and their binding areas on voltage-gated sodium channels. *Front. Pharmacol.* 2:71. doi: 10.3389/fphar.2011.00071
- Terrenoire, C., Wang, K., Tung, K. W., Chung, W. K., Pass, R. H., Lu, J. T., et al. (2013). Induced pluripotent stem cells used to reveal drug actions in a long QT syndrome family with complex genetics. *J. Gen. Physiol.* 141, 61–72. doi: 10.1085/jgp.201210899
- Toraason, M., Luken, M. E., Breitenstein, M., Krueger, J. A., and Biagini, R. E. (1989). Comparative toxicity of allylamine and acrolein in cultured myocytes and fibroblasts from neonatal rat heart. *Toxicology* 56, 107–117. doi: 10.1016/0300-483X(89)90216-3
- Veeraman, C. C., Kosmidis, G., Mummery, C. L., Casini, S., Verkerk, A. O., and Bellin, M. (2015). Immaturity of human stem-cell-derived cardiomyocytes in culture: fatal flaw or soluble problem? *Stem Cells Dev.* 24, 1035–1052. doi: 10.1089/scd.2014.0533
- Wang, D. W., Yazawa, K., Makita, N., George, A. L. Jr., and Bennett, P. B. (1997). Pharmacological targeting of long QT mutant sodium channels. *J. Clin. Invest.* 99, 1714–1720. doi: 10.1172/JCI119335
- Wang, Z., Ferrmini, B., and Nattel, S. (1993). Sustained depolarization-induced outward current in human atrial myocytes. Evidence for a novel delayed rectifier K⁺ current similar to Kv1.5 cloned channel currents. *Circ. Res.* 73, 1061–1076. doi: 10.1161/01.RES.73.6.1061
- Waring, M. J., Arrowsmith, J., Leach, A. R., Leeson, P. D., Mandrell, S., Owen, R. M., et al. (2015). An analysis of the attrition of drug candidates from four major pharmaceutical companies. *Nat. Rev. Drug Discov.* 14, 475–486. doi: 10.1038/nrd4609
- Wills, L. P., Trager, R. E., Beeson, G. C., Lindsey, C. C., Peterson, Y. K., Beeson, C. C., et al. (2012). The beta2-adrenoceptor agonist formoterol stimulates mitochondrial biogenesis. *J. Pharmacol. Exp. Ther.* 342, 106–118. doi: 10.1124/jpet.112.191528
- Woodford, C. R., Frady, E. P., Smith, R. S., Morey, B., Canzi, G., Palida, S. F., et al. (2015). Improved PeT molecules for optically sensing voltage in neurons. *J. Am. Chem. Soc.* 137, 1817–1824. doi: 10.1021/ja510602z
- Yang, P., Kanki, H., Drolet, B., Yang, T., Wei, J., Viswanathan, P. C., et al. (2002). Allelic variants in long-QT disease genes in patients with drug-associated torsades de pointes. *Circulation* 105, 1943–1948. doi: 10.1161/01.CIR.0000014448.19052.4C
- Yang, X., Rodriguez, M., Pabon, L., Fischer, K. A., Reinecke, H., Regnier, M., et al. (2014). Tri-iodo-L-thyronine promotes the maturation of human cardiomyocytes-derived from induced pluripotent stem cells. *J. Mol. Cell. Cardiol.* 72, 296–304. doi: 10.1016/j.yjmcc.2014.04.005
- Zeng, H., Roman, M. I., Lis, E., Lagrutta, A., and Sannajust, F. (2016). Use of FDSS/muCell imaging platform for preclinical cardiac electrophysiology safety screening of compounds in human induced pluripotent stem cell-derived cardiomyocytes. *J. Pharmacol. Toxicol. Methods* 81, 217–222. doi: 10.1016/j.vascn.2016.05.009

Conflict of Interest Statement: JP is a founder and MM is on the scientific advisory board of Vala Sciences, and both have equity in the company, which manufactures a high content instrument used in these studies.

The other author declares that the research was conducted in the absence of any commercial or financial relationships that could be construed as a potential conflict of interest.

The reviewer SC and handling Editor declared their shared affiliation, and the handling Editor states that the process nevertheless met the standards of a fair and objective review.

Copyright © 2017 McKeithan, Savchenko, Yu, Cerignoli, Bruyneel, Price, Colas, Miller, Cashman and Mercola. This is an open-access article distributed under the terms of the Creative Commons Attribution License (CC BY). The use, distribution or reproduction in other forums is permitted, provided the original author(s) or licensor are credited and that the original publication in this journal is cited, in accordance with accepted academic practice. No use, distribution or reproduction is permitted which does not comply with these terms.